Monbusho Grant-in-Aids for Scientific Research, nos. 03042052 and 06750025.

References

AFANASEV, A. M., IMAMOV, R. M., MASLOV, A. V. & MUKHAMEDZHANOV, E. KH. (1989). *Phys. Status Solidi A*, **113**, K153–K155.

AUTHIER, A. (1986). *Acta Cryst.* A**42**, 414–426.

BATTERMAN, B. W. & COLE, H. (1964). *Rev. Mod. Phys.* **36**, 681–717.

BRINGANS, R. D. (1992). *Crit. Rev. Solid State Mater. Sci.* **17**, 353–395.

COPEL, M., TROMP, R. M. & KÖHLER, U. K. (1988). *Phys. Rev. B*, **37**, 10756–10763.

COWAN, P. L. (1985). *Phys. Rev. B*, **32**, 5437–5439.

COWAN, P. L., BRENNAN, S., JACH, T., BEDZYK, M. J. & MATERLIK, G. (1986). *Phys. Rev. Lett.* **57**, 2399–2402

HASHIZUME, H. & SAKATA, O. (1989*a*). *J. Phys. (Paris) Colloq.* C7, *Suppl.* 10, **50**, 225–229.

HASHIZUME, H. & SAKATA, O. (1989*b*). *Rev. Sci. Instrum.* **60**, 2373–2375.

HEADRICK, R. L. & GRAHAM, W. R. (1988). *Phys. Rev. B*, **37**, 1051–1054.

ISHIZAKA, A. & SHIRAKI, Y. (1986). *J. Electrochem. Soc.* **133**, 666–671.

JACH, T. & BEDZYK, M. J. (1990). *Phys. Rev. B*, **42**, 5399–5402.

JACH, T. & BEDZYK, M. J. (1993). *Acta Cryst.* A**49**, 346–350.

JACH, T., COWAN, P. L., SHEN, Q. & BEDZYK, M. J. (1989). *Phys. Rev. B*, **39**, 5739–5747.

NAKAYAMA, K., TANAKA, M., ANNAKA, S., SUGII, K., TAKAHASHI, T., KIKUTA, S., ISHIKAWA, T., ANDO, M. & KOHRA, K. (1986). *X-ray Instrumentation for the Photon Factory: Dynamic Analysis of Microstructures in Matter*, edited by S. HOSOYA, Y. IITAKA & H. HASHIZUME, pp. 269–274. Tokyo: KTK Science.

OLMSTEAD, M. A., BRINGANS, R. D., UHRBERG, R. I. G. & BACHRACH, R. Z. (1986). *Phys. Rev. B*, **34**, 6041–6044.

PATEL, J. R. & GOLOVCHENKO, J. A. (1983). *Phys. Rev. Lett.* **50**, 1858–1861.

PATEL, J. R., GOLOVCHENKO, J. A., FREELAND, P. E. & GOSSMANN, H. J. (1987). *Phys. Rev. B*, **36**, 7715–7717.

ROBINSON, I. K. (1991). *Handbook on Synchrotron Radiation*, Vol. 3, edited by G. S. BROWN & D. E. MONCTON, pp. 221–266. Amsterdam: North-Holland.

SAITOH, Y., HASHIZUME, H. & TSUTSUI, K. (1988). *Jpn. J. Appl. Phys.* **27**, 1386–1396.

SAKATA, O. (1994). Thesis, Tokyo Institute of Technology, Japan.

SAKATA, O. & HASHIZUME, H. (1987). Rep. RLEMTIT, Vol. 12, pp. 45–57. Tokyo Institute of Technology, Japan.

SAKATA, O. & HASHIZUME, H. (1988). *Jpn. J. Appl. Phys.* **27**, L1976–L1979.

SAKATA, O. & HASHIZUME, H. (1991). Rep. RLEMTIT, Vol. 16, pp. 27–38. Tokyo Institute of Technology, Japan.

SAKATA, O. & HASHIZUME, H. (1995). *Rev. Sci. Instrum.* In the press.

SAKATA, O., HASHIZUME, H. & KURASHINA, H. (1993). *Phys. Rev. B*, **48**, 11408–11411.

SAKATA, O., KAWAMOTO, I. & HASHIZUME, H. (1992). Conference of the Asian Crystallographic Association, AsCA '92, 16Q-08, Singapore, 13–16 November 1992. Collected Abstracts.

Acta Cryst. (1995). A**51**, 384–390

Computing Accurate Bragg Diffraction Intensities by Simulation

BY E. RITTGER*

SBPM-DBCM-DSV, CEA-Centre d'Etudes Nucléaires de Saclay, F-91191 Gif sur Yvette CEDEX, France

(*Received* 5 *July* 1994; *accepted* 3 *January* 1995)

Abstract

The diffraction intensities obtained from a computer simulation of a crystal exhibit substantial finite-size effects and converge only very slowly to the thermodynamic limit when the simulation box is enlarged. Two procedures that improve the convergence by correcting for this effect are compared. One of them, the elasticity-tensor correction, is shown to yield highly accurate results with a small simulation box.

1. Introduction

The harmonic approximation of the Hamiltonian is a general and analytically convenient concept for studying the thermal and mechanical properties of crystalline substances at low temperature. It explains diffraction intensities in terms of averaged atomic positions and fluctuations and forms the basis for structure determination even when harmonicity is only a poor approximation. At high temperatures, however, when the system explores anharmonic regions of its phase space, it may not be good enough, especially if a system is to be studied in more detail than just a mean structure and temperature factors. Besides this, some crystals that contain liquids, *e.g.* protein crystals containing water, are not amenable to theories that allow atoms only to vibrate around mean positions. In such cases, computer simulation is nowadays the best tool. It is therefore desirable to have a general recipe for computing accurate theoretical diffraction intensities for a given potential-energy function by simulation.

Two theoretical concepts for such a recipe, the 'quasi-harmonic correction' and the 'elasticity-tensor correction' are presented in §§ 2 and 3. To test them, they are applied to a simple model described in § 4. The test results are shown and compared in §§ 5 and 6. § 7 gives a summary.

* Present address: Osnabruecker Strasse 22, D-10589 Berlin, Germany.

2. Basics and the quasi-harmonic correction

The Bragg diffraction intensity for X-rays is given by

$$I_{\mathrm{Br}}(\mathbf{k}) = |\langle \tilde{f}(\mathbf{k})\rangle|^2 \tag{1}$$

in terms of the thermal average of the Fourier transform

$$\tilde{f}(\mathbf{k}) = \sum_{li} \tilde{f}_i(\mathbf{k}) \exp(-i\,\mathbf{k}\mathbf{r}_{li}) \tag{2}$$

of the electron density

$$f(\mathbf{r}) = \sum_{li} f_i(\mathbf{r} - \mathbf{r}_{li}) \tag{3}$$

or, equivalently, by

$$I_{\mathrm{Br}}(\mathbf{k}) = |F(\mathbf{k})|^2 N \Delta(\mathbf{k}) \tag{4}$$

in terms of the structure factor $F(\mathbf{k})$ and

$$\Delta(\mathbf{k}) = \begin{cases} N & \text{if } \mathbf{k} \text{ is a reciprocal vector} \\ 0 & \text{otherwise.} \end{cases} \tag{5}$$

Here and below, the indices $l, m, n = 1, \ldots, N$ enumerate the unit cells, $i, j = 1, \ldots, n$ enumerate the n atoms in a unit cell, $\tilde{f}_i(\mathbf{k})$ is the form factor for atom type i and $\mathbf{k}$ is the wave vector. The position

$$\mathbf{r}_{li} = \mathbf{r}_l + \mathbf{s}_i + \mathbf{u}_{il} \tag{6}$$

of atom i in cell l can be decomposed into the position $\mathbf{r}_l$ of the origin of the coordinate frame of cell l, the average position $\mathbf{s}_i$ of atom i in this cell and coordinate frame and the deviation $\mathbf{u}_{il}$ from this average position.

For a classical harmonic crystal with potential energy

$$\Phi = \tfrac{1}{2} \sum_{limj} \mathbf{u}_{il}^T \Phi_{il,jm} \mathbf{u}_{jm}, \tag{7}$$

where the $\Phi_{il,jm}$ are 3×3 matrices of force constants, canonical averaging of (2) leads to the structure factor

$$\begin{aligned} F(\mathbf{k}) &= \sum_i F_i(\mathbf{k}) \\ &= \sum_i \tilde{f}_i(\mathbf{k}) \exp(-i\,\mathbf{k}\mathbf{s}_i - \mathbf{k}^T U_{iN} \mathbf{k}/2). \end{aligned} \tag{8}$$

Here, the 3×3 matrix of mean square fluctuations

$$U_{iN} = \langle \mathbf{u}_{il} \mathbf{u}_{il}^T \rangle = (kT/N) \sum_{\mathbf{q}} [\tilde{\Phi}(\mathbf{q})]_{ii}^{-1} \tag{9}$$

is computed from the $3n \times 3n$ matrix $\tilde{\Phi}(\mathbf{q})$, which consists of the 3×3 submatrices

$$\tilde{\Phi}_{ij}(\mathbf{q}) = \sum_l \Phi_{il,jm} \exp[-i\mathbf{q}(\mathbf{r}_l - \mathbf{r}_m)]$$

$$i, j = 1, \ldots n; \text{ all } m. \tag{10}$$

This matrix $\tilde{\Phi}(\mathbf{q})$ is inverted. The ii submatrix of the inverse is averaged over all wave vectors $\mathbf{q}$ of the harmonic modes of the crystal and multiplied by kT. For a macroscopic crystal with volume V, the sum over the modes can be replaced by an integral over the Brillouin zone (BZ):

$$U_{i\infty} = kTV/(2\pi)^3 N \int_{\mathrm{BZ}} [\tilde{\Phi}(\mathbf{q})]_{ii}^{-1} \, \mathrm{d}^3 q. \tag{11}$$

This is precisely where the simulation has its shortcoming. The periodic boundary conditions will permit only a few discrete modes. An integer multiple of their wavelength must fit exactly in the simulation box. All other modes are suppressed. Consequently, a simulation will yield diffraction intensities corresponding to (9) rather than to (11). In other words, a simulation will not lead directly to correct results, not even for a harmonic system. Fig. 1 shows why the error may be large. The integrand in (11) diverges as q^{-2} for $\mathbf{q} \to \mathbf{0}$, whereas the values of the integrand at the discrete $\mathbf{q}$ values of (9) lead to a poor approximation of (11), which does not contain the large contribution near $\mathbf{q} = \mathbf{0}$.

To correct for this error, we assume that, for any given (non-harmonic) system, the relation between the exact structure factors $F_i(\mathbf{k})$ and their simulated counterparts $F_{i,\mathrm{sim}}(\mathbf{k})$ is roughly the same as for some harmonic approximation to the real system, *i.e.*

$$F_i(\mathbf{k})/F_{i,\mathrm{sim}}(\mathbf{k}) \simeq F_{i\infty}^{\mathrm{harm}}(\mathbf{k})/F_{iN}^{\mathrm{harm}}(\mathbf{k}). \tag{12}$$

The right-hand side of (12), *i.e.* the relation of the harmonic structure factors computed with (11) and (9), respectively, then constitutes a correction factor for the simulation results. Since the correction arises mainly from long-wavelength acoustic modes, where all atoms in a unit cell perform the same motion, we can, of course, expect the correction factors (12) to be very nearly identical for all atoms.

In search of a harmonic approximation that gives good correction factors, we compare two concepts: the quasi-harmonic correction and the elasticity-tensor correction. The quasi-harmonic correction results from the harmonic theory outlined above, except that the simulation average of the second derivatives of the potential energy replaces the matrix $\Phi_{il,jm}$ in (7). By means of (8), the quasi-harmonic (qh) correction factor for the Bragg intensities then becomes

$$|F_{i\infty}^{\mathrm{qh}}(\mathbf{k})/F_{iN}^{\mathrm{qh}}(\mathbf{k})|^2 = \exp[-\mathbf{k}^T (U_{i\infty}^{\mathrm{qh}} - U_{iN}^{\mathrm{qh}})\mathbf{k}]. \tag{13}$$

3. The elasticity-tensor correction

The elasticity-tensor correction is based on a more macroscopic approach. The whole crystal is regarded as a continuum, of which the volume element at $\mathbf{r}$ is displaced to $\mathbf{r} + \mathbf{u}(\mathbf{r})$ by a thermal fluctuation $\mathbf{u}(\mathbf{r})$. The long-wavelength part of these fluctuations is precisely what the simulation suppresses but it can be described by means of the macroscopic elasticity tensor

$$C_{\alpha\beta\gamma\delta} := (1/V)(\partial^2 A / \partial S_{\alpha\beta} \, \partial S_{\gamma\delta}), \tag{14}$$

where A denotes the (Helmholtz) free energy of a system with volume V and $S_{\alpha\beta}$ describes a linear deformation

$$x_\alpha \to x'_\alpha = S_{\alpha\beta} x_\beta. \tag{15}$$

Here and below, Greek indices denote Cartesian coordinates and are summed over when they occur twice in a product. A fluctuation formula for the elasticity tensor is derived in the Appendix.

The above definition of the elasticity tensor is based on a linear deformation (15) of a macroscopic crystal, which we can also conceive as a volume element of a still larger crystal, at least as long as the wavelength of the deformation is much greater than the nearest-neighbour interatomic distances. The deformation matrix

$$S = \mathbf{1} + \partial \mathbf{u}/\partial \mathbf{r} \tag{16}$$

would then be the locally linear approximation to the more general deformation $\mathbf{u}(\mathbf{r})$ introduced above. To obtain the total free energy of the deformation, one expands the free energy of each volume element in a Taylor series up to second order and sums over all volume elements. Since areas of compression and expansion compensate for each other in first order, the free energy of deformation is

$$\delta^2 A = \tfrac{1}{2} \int \delta S_{\alpha\beta} C_{\alpha\beta\gamma\delta} \delta S_{\gamma\delta} \, \mathrm{d}^3 r = \tfrac{1}{2} \int (\partial_\beta u_\alpha) C_{\alpha\beta\gamma\delta} (\partial_\delta u_\gamma) \, \mathrm{d}^3 r. \tag{17}$$

Using Parseval's theorem, we can replace $\mathbf{u}(\mathbf{r})$ by its Fourier transform $\tilde{\mathbf{u}}(\mathbf{q})$,

$$\delta^2 A = \tfrac{1}{2} \int C_{\alpha\beta\gamma\delta} q_\beta q_\delta \tilde{u}^*_\alpha \tilde{u}_\gamma \, \mathrm{d}^3 q. \tag{18}$$

This means that, for each mode $\mathbf{q}$, the associated free energy

$$A(\mathbf{q}) = \tfrac{1}{2} G_{\alpha\gamma}(\mathbf{q}) \tilde{u}^*_\alpha \tilde{u}_\gamma \tag{19}$$

is proportional to the square of the ampitude with a proportionality constant

$$G_{\alpha\gamma}(\mathbf{q}) = C_{\alpha\beta\gamma\delta} q_\beta q_\delta. \tag{20}$$

With the probability distribution of the amplitude proportional to $\exp[-A(\mathbf{q})/kT]$, we get, for the mean square fluctuation,

$$\langle \tilde{u}^*_\alpha \tilde{u}_\gamma \rangle = kT G^{-1}_{\alpha\gamma}(\mathbf{q}). \tag{21}$$

Since in a thermal ensemble all modes contribute independently to a displacement $\mathbf{u}(\mathbf{r})$, we get for the mean square displacement at any $\mathbf{r}$, analogously to (11),

$$[U^{\mathrm{et}}_\infty]_{\alpha\gamma} = \langle u_\alpha u_\gamma \rangle = [kT/(2\pi)^3] \int G^{-1}_{\alpha\gamma}(\mathbf{q}) \, \mathrm{d}^3 q. \tag{22}$$

Introducing spherical coordinates (q, θ, φ) in $\mathbf{q}$ space, we can factorize

$$G^{-1}(\mathbf{q}) = H^{-1}(\theta, \varphi) q^{-2}, \tag{23}$$

integrate over q from zero to some $q_m(\theta, \varphi)$, to be determined later, and obtain

$$U^{\mathrm{et}}_\infty = [kT/(2\pi)^3] \int_0^\pi \sin\theta \, \mathrm{d}\theta \int_0^{2\pi} H^{-1}(\theta, \varphi) q_m(\theta, \varphi) \, \mathrm{d}\varphi. \tag{24}$$

In this elasticity tensor (et) approximation, the mean square displacement due to the simulated modes would be

$$U^{\mathrm{et}}_N = (kT/V) \sum_{\mathbf{q}} G^{-1}(\mathbf{q}), \tag{25}$$

which is analogous to (9) and where the sum is over the simulated modes that lie in the integration range in (22). Since only that part of $C_{\alpha\beta\gamma\delta}$ that is symmetric in β and δ contributes to (20), it follows from the discussion in the Appendix that G and H and hence their inverses are symmetric. For the computation of (24), we split

$$C_{\alpha\beta\gamma\delta} = C^E_{\alpha\beta\gamma\delta} - \delta_{\alpha\gamma} P_{\beta\delta} \tag{26}$$

in the two parts shown, again following the discussion in the Appendix. For an unstrained crystal with isotropic pressure tensor $P_{\beta\delta} = \delta_{\beta\delta} P$, we obtain

$$G_{\alpha\gamma}(\mathbf{q}) = C^E_{\alpha\beta\gamma\delta} q_\beta q_\delta - \delta_{\alpha\gamma} p q^2. \tag{27}$$

We can now use the fact that only the symmetric part of $C^E_{\alpha\beta\gamma\delta}$ contributes to (27) and that this part is invariant under any permutation of its indices (see Appendix). Thus, we need to compute, apart from the pressure p, at most 15 independent components. This number can be further reduced by the symmetry of the crystal.

Since this continuum model is adequate only for small $\mathbf{q}$, it might be inappropriate to extend the ranges of integration in (22) and summation in (25) over the whole Brillouin zone of the crystal. The minimum range is certainly the Brillouin zone of the simulation box (see Fig. 1), which contains the largest part of the correction. All modes in this range are completely suppressed in the simulation and $U^{\mathrm{et}}_N = 0$. The next larger range would be one that contains one layer of simulated modes (26 in three dimensions) around the minimum range ($|q_x| < 3\pi/L$ in Fig. 1). One can also include more layers in the computation of the correction factor

$$|F^{\mathrm{et}}_\infty(\mathbf{k})/F^{\mathrm{et}}_N(\mathbf{k})|^2 = \exp[-\mathbf{k}^T (U^{\mathrm{et}}_\infty - U^{\mathrm{et}}_N) \mathbf{k}], \tag{28}$$

but only a test of the results will tell whether the inclusion of more modes with shorter wavelengths, for which the elasticity tensor is not strictly valid, will still improve the results. Note, however, that, for a fixed shape of the range, q_m and hence (24) are inversely proportional to some linear dimension L of the simulation box and that, for a fixed number m of layers, the same is true for (25). Thus, for any m, the correction factor (28) can be written

$$|F^{\mathrm{et}}_\infty(\mathbf{k})/F^{\mathrm{et}}_N(\mathbf{k})|^2 = \exp[-\mathbf{k}^T \chi_m \mathbf{k}/L], \tag{29}$$

where $\chi_m = L(U_\infty^{\text{et}} - U_N^{\text{et}})$ does not depend on the size of the simulation box. This reveals the power law for extrapolation.

In the following, the computation of (24) is outlined for a cubic crystal. In this case, only two independent components contribute to (27), namely

$$a = \tfrac{1}{3}(C^E_{xxxx} + C^E_{yyyy} + C^E_{zzzz}) \tag{30}$$

and

$$b = \tfrac{1}{18}\sum_{\alpha\neq\beta}(C^E_{\alpha\alpha\beta\beta} + C^E_{\alpha\beta\alpha\beta} + C^E_{\alpha\beta\beta\alpha}). \tag{31}$$

This leads to

$$G_{\alpha\gamma}(\mathbf{q}) = 2bq_\alpha q_\gamma + \delta_{\alpha\gamma}[(a-3b)q_\alpha^2 + (b-p)q^2], \tag{32}$$

which can be inverted analytically. Since a second-rank tensor with cubic symmetry is isotropic, we only need to know the trace of the inverse. In spherical coordinates, we get

$$\begin{aligned}\operatorname{Tr} H^{-1} = {} & [(b-p)(b-3p+2a) + (a-3b)(a+b) \\ & \times (\sin^4\theta\cos^2\varphi\sin^2\varphi + \cos^2\theta\sin^2\theta)]/D,\end{aligned} \tag{33}$$

$$\begin{aligned}D = {} & (b-p)^2(a-p) + (a-3b)^2(a+3b) \\ & \times \sin^4\theta\cos^2\varphi\sin^2\varphi\cos^2\theta \\ & + (b-p)(a-3b)(a+b) \\ & \times (\sin^4\theta\cos^2\varphi\sin^2\varphi + \cos^2\theta\sin^2\theta).\end{aligned}$$

The integration range is delimited by

$$\begin{aligned}q_m(\theta,\varphi) = {} & (1+2m)(\pi/L)\min(|\sin\theta\cos\varphi|^{-1}, \\ & |\sin\theta\sin\varphi|^{-1}, |\cos\theta|^{-1}),\end{aligned} \tag{34}$$

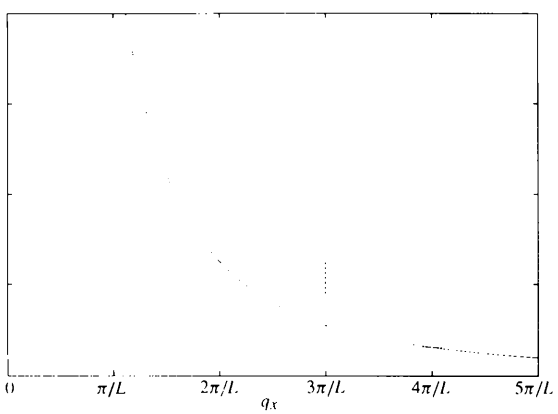

Fig. 1. Contributions of harmonic modes $\mathbf{q}$ to the mean square fluctuations qualitatively. For a simulation box of length L along the x axis, simulated modes are at $q_x = 2\pi\nu/L$, $\nu = 1, 2, \ldots, \leq N/2$. —— Integrand of (11); - - - - discrete-modes approximation of the integrand that yields the estimate (9) of (11). The Brillouin zone of the simulation box is delimited by $q_x = \pm\pi/L$.

Table 1. *Some results of the simulations: N is the number of atoms, a and b are defined in (30) and (31), respectively, p is the isotropic pressure, χ_m is defined in (29)*

All data are in 'Lennard–Jones units'.

N	6912	2048	864	256
MC steps per atom	8000	10800	12800	21600
Quasi-harmonic correction				
Tr $U_{i\infty}/3\,(10^{-3}\sigma^2)$ (equation 11)	6.500	6.503	6.511	6.525
Tr $U_{iN}/3\,(10^{-3}\sigma^2)$ (equation 9)	6.164	5.996	5.831	5.500
Tr $(U_{i\infty} - U_{iN})/3\,(10^{-3}\sigma^2)$	0.336	0.507	0.680	1.025
Elasticity-tensor correction				
$a\,(\varepsilon\sigma^{-3})$	48.0	51.0	48.5	50.0
$b\,(\varepsilon\sigma^{-3})$	28.5	29.1	28.5	29.0
$p\,(\varepsilon\sigma^{-3})$	1.81	1.81	1.80	1.79
$\chi_0\,(10^{-3}\sigma^3)$	6.94	6.47	6.85	6.61
$\chi_1\,(10^{-3}\sigma^3)$	7.73	7.29	7.56	7.42
$\chi_2\,(10^{-3}\sigma^3)$	7.97	7.51	7.90	7.65

where $L = V^{1/3}$ is the length of the simulation box. For $m = 0$, it is the Brillouin zone of the simulation box. For $m > 0$, it also includes m layers of simulated modes.

4. Simulations

To test the correction methods of the previous sections, they were applied to a series of Monte Carlo simulations of f.c.c. Lennard–Jones crystals with various box sizes. Temperature and volume were chosen in the crystal region of the phase diagram (Luckas, Lucas, Deiters & Gubbins, 1986), not far from the solid–liquid transition ($kT = 0.75\varepsilon$ and $V/N = 1.02\sigma^3$ in terms of the Lennard–Jones parameters ε and σ). The cut-off distance was 2.75σ and the maximum step size was adjusted to give roughly 50% acceptance rate. Several thousand steps per atom were performed for equilibration. Then, every ten steps per atom, a configuration was recorded for computing the averages. Besides the structure factors for the Miller indices 100 and 544, the virial, the expressions needed for the elasticity tensor (see Appendix) and the Hessian of the potential energy were also averaged. More details on the simulations are given in Table 1.

For the calculation of the canonical average of (2), the atomic form factors were set to unity for simplicity. Note that (2) depends on the origin of the coordinate frame, which one usually sets at the centre of mass in a molecular dynamics simulation. In a Monte Carlo simulation, the centre of mass drifts randomly and each configuration has to be shifted back to prevent this drift from averaging out the structure in the long run.

To characterize the anharmonicity of the test system, the Hessian of the potential was determined for the perfect f.c.c. crystal at $T = 0$ and a mean square fluctuation (11) of $\operatorname{Tr} U_{i\infty}/3 = 0.0193\sigma^2$ was calculated from this for $kT = 0.75\varepsilon$. This constitutes the harmonic aproximation result. Furthermore, a short simulation with 256 atoms was run at $kT = 0.10\varepsilon$ to obtain an average of

the Hessian at this low temperature. The mean square fluctuation calculated from this for $kT = 0.75\varepsilon$ is $\mathrm{Tr}\, U_{i\infty}/3 = 0.0146\sigma^2$. The quasi-harmonic approximation result from the Hessians averaged at $kT = 0.75\varepsilon$ (see Table 1) is $\mathrm{Tr}\, U_{i\infty}/3 = 0.0065\sigma^2$. Since these results should be identical for a truly harmonic system, the discrepancy of a factor of three between them reveals the pronounced anharmonicity of the test system.

5. Results for the harmonic potential theories

The uncorrected simulation results for the 100 reflection are plotted in Fig. 2 *versus* L^{-1} as suggested by the power law for extrapolation established above. One can see, on one side, that the size dependence is considerable. On the other side, the power law is well obeyed and the straight-line fit extrapolates the data to $-\ln|F_{100}|^2 = 0.3158$ for $L = \infty$. By contrast, the quasi-harmonic approximation, with Hessians averaged at $kT = 0.75\varepsilon$, yields results that hardly depend on size and extrapolate to $-\ln|F_{100}|^2 = 0.3010$. This is already a great improvement over the harmonic approximation of the previous section, which would yield $-\ln|F_{100}|^2 = 0.895$, but it still means a 1.5% overestimation of the Bragg intensity I_{Br} of the lowest-order reflection.

Applying the quasi-harmonic correction factor (13) computed from each simulation to the results reduces their size dependence considerably. Furthermore, all values obtained are better than the quasi-harmonic approximation and they extrapolate to the correct limit (see Fig. 2). For the 544 reflection, Fig. 3 shows that the situation is essentially the same. Note that the extra-polated quasi-harmonic value of I_{Br} is 12.5% to high.

6. Results of the elasticity-tensor correction

In each simulation, the pressure and the elastic constants (30) and (31), shown in Table 1, were calculated as

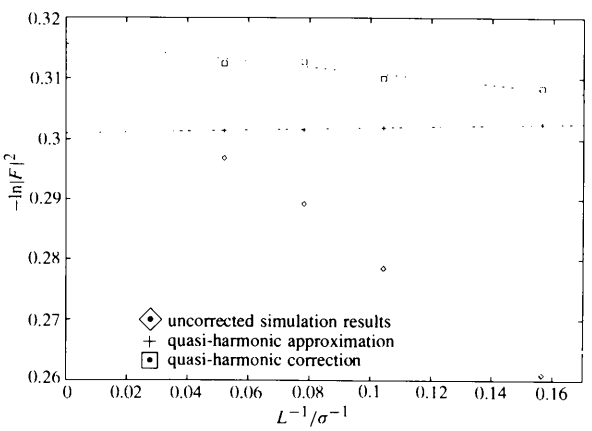

Fig. 2. Results of harmonic potential theories for Miller indices 100 and for the four box sizes of Table 1. The straight lines are least-squares fits to the data.

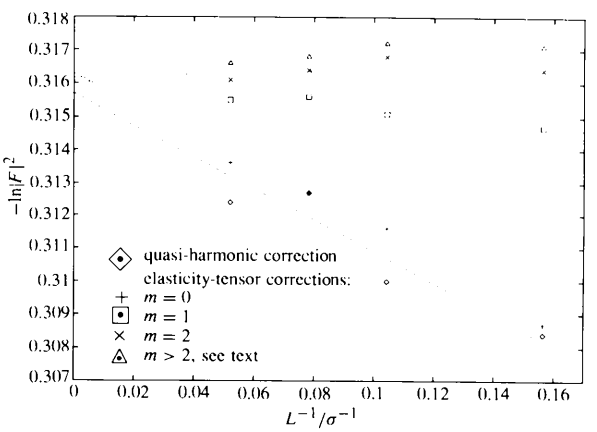

Fig. 4. Results of elasticity tensor corrections for Miller indices 100 and for the four box sizes of Table 1. The straight lines are least-squares fits to the data.

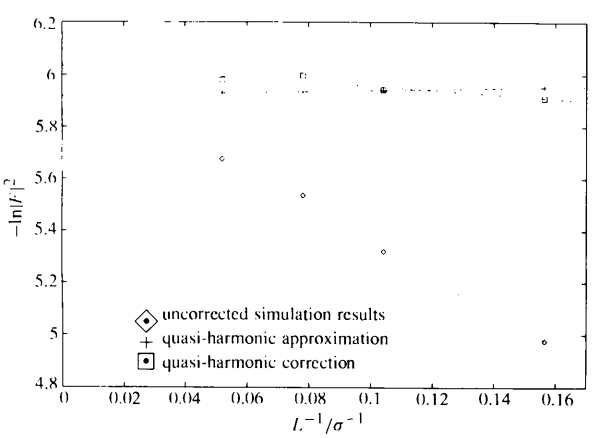

Fig. 3. Same as Fig. 2 but for Miller indices 544.

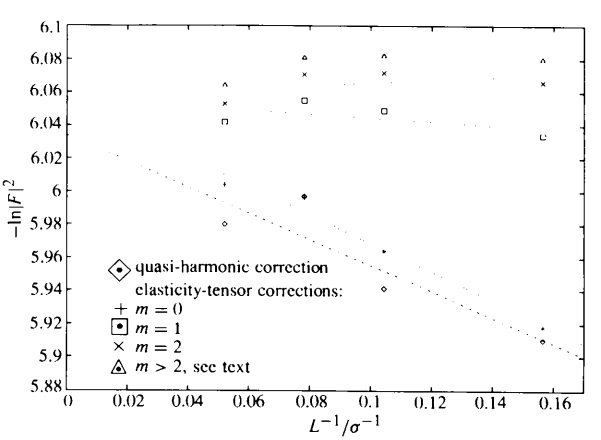

Fig. 5. Same as Fig. 4 but for Miller indices 544.

outlined in the Appendix. Then correction factors (28) were computed for ranges of integration in (22) and summation in (25) that contain $m = 0, 1, 2, \ldots$ layers of simulated modes. The χ_m (29) are reported in Table 1. The corrected results for the 100 reflection are compared with those of the quasi-harmonic correction in Fig. 4 on a magnified scale. While the values for $m = 0$ are close to the quasi-harmonic ones, those for $m \geq 1$ are all much better and extrapolate to $-\ln|F_{100}|^2 = 0.3161$ in excellent agreement with the previous section. The perfect correction seems to lie between $m = 1$ and $m = 2$. The intensities estimated with $m = 1$ or $m = 2$ are all within 0.15% of the extrapolated value, which represents an amazing accuracy. With $m > 2$, these values overcompensate the box-size dependence of the uncorrected simulation results. Obviously, the elasticity tensor is not appropriate at the shorter wavelengths that they take into account. The remaining results shown in Fig. 4 are for the maximum m for which the integration range in (22) is still entirely within the Brillouin zone of the f.c.c. crystal. They are still very good estimates, though not the best ones.

The results for the 544 reflection are shown in Fig. 5. They are completely analogous. For $m \geq 1$, all the estimated intensities are within 2.5% of the extrapolated value.

7. Concluding remarks

The results of the two previous sections have shown that both methods reduce the finite-size dependence of simulated diffraction intensities considerably. In contrast to the quasi-harmonic approximation, they can be extrapolated to the same infinite-size limit as the uncorrected simulation results using the power law based on the same theory. The accuracy of a one-simulation result is, however, much better for the elasticity-tensor correction method. Even for the very anharmonic system studied here and for only 256 atoms, the errors in the diffraction intensities are only 0.15% for a low-order and 2.5% for a high-order reflection. One possible explanation for this is that the free energy as a function of deformation is more harmonic than the potential energy as a function of particle positions. Concerning the best choice for the number m of layers of simulated modes in the correction formula in applications where only one simulation is to be performed, the following recipe is proposed: compute the values for $m = 1$ and $m = 2$ and take the mean if the two values agree within the desired accuracy.

There is also an important conceptual aspect that deserves mentioning. For very large unit cells, *e.g.* protein crystals, the quasi-harmonic theories involve very large matrices and become impractical. In the elasticity-tensor method, it is always a 3×3 matrix that is inverted and the number of elastic constants needed never exceeds 15. Furthermore, if there is liquid water between protein molecules, the quasi-harmonic theories, which require each atom to have an equilibrium position around which it can only vibrate, are not applicable. For the elasticity-tensor method, this does not pose a problem.

APPENDIX
Elasticity tensors

The fluctuation formula for the elasticity tensor (14) can be derived from the free energy $A = -kT \ln Q$ and the partition function

$$Q = Q_k \int \exp[-\Phi(\ldots \mathbf{r}'_{li} \ldots)/kT] (\mathrm{d}x')^{3nN} \tag{35}$$

of a deformed crystal, where Q_k is the kinetic part of Q and the integration extends over the deformed volume of the crystal. Integrating over the undeformed volume by returning to the unprimed coordinates introduces the transformation (15) as a set of variables:

$$Q = Q_k \int \exp[-\Phi(\ldots S\mathbf{r}_{li} \ldots)/kT] (\det S)^{nN} (\mathrm{d}x)^{3nN}. \tag{36}$$

To obtain the derivatives, one needs

$$\partial(\det S)/\partial S_{\alpha\beta} = (\det S)(S^{-1})_{\beta\alpha}, \tag{37}$$

which can be proven starting from the definition of the determinant as the sum over all permutations P with sign $(P) = +1$ (-1) for an even (odd) permutation:

$$\begin{aligned} \partial(\det S)/\partial S_{\alpha\beta} &= \partial\left[\sum_P \mathrm{sign}(P) \prod_\mu S_{\mu P(\mu)}\right]\Big/ \partial S_{\alpha\beta} \\ &= \sum_{P:P(\alpha)=\beta} \mathrm{sign}(P) \prod_{\mu:\mu\neq\alpha} S_{\mu P(\mu)}. \end{aligned} \tag{38}$$

Since, for the permutations P summed over here, $\mathrm{sign}(P) = (-1)^{\alpha+\beta}\mathrm{sign}(P')$, where P' is a permutation of the indices of the submatrix $M^{\alpha\beta}$ (which excludes the row α and the column β), (38) becomes

$$\partial(\det S)/\partial S_{\alpha\beta} = (-1)^{\alpha+\beta} \det M^{\alpha\beta}. \tag{39}$$

Comparison of this with the formula for the inverse,

$$S^{-1}_{\beta\alpha} = (\det S)^{-1}(-1)^{\alpha+\beta} \det M^{\alpha\beta}, \tag{40}$$

leads directly to (37). With this result, one obtains for the first derivatives

$$\partial A/\partial S_{\alpha\beta} = -(S^{-1})_{\beta\gamma} V P_{\gamma\alpha}, \tag{41}$$

where

$$V P_{\gamma\alpha} = nNkT\delta_{\gamma\alpha} - \left\langle \sum_{li} x'_{\gamma li}\, \partial\Phi/\partial x'_{\alpha li} \right\rangle \tag{42}$$

is the volume times the pressure tensor. Using

$$\mathrm{d}S^{-1}_{\beta\alpha} = -S^{-1}_{\beta\mu}\, \mathrm{d}S_{\mu\nu}\, S^{-1}_{\nu\alpha}, \tag{43}$$

which can easily be proven by multiplying the differential of the unit matrix

$$0 = \mathrm{d}\mathbf{1} = \mathrm{d}(S^{-1}S) = (\mathrm{d}S^{-1})S + S^{-1}\,\mathrm{d}S \qquad (44)$$

by S^{-1} from the right, we get, for the second derivatives at $S = \mathbf{1}$,

$$\begin{aligned}\partial^2 A/\partial S_{\alpha\beta}\partial S_{\gamma\delta} &= nNkT\delta_{\beta\gamma}\delta_{\alpha\delta} \\ &\quad + \left\langle \sum_{li,\,mj} x_{\delta li}(\partial^2\Phi/\partial x_{\gamma li}\,\partial x_{\alpha mj})x_{\beta mj}\right\rangle \\ &\quad - (1/kT)[\langle\Psi_{\alpha\beta}\Psi_{\gamma\delta}\rangle - \langle\Psi_{\alpha\beta}\rangle\langle\Psi_{\gamma\delta}\rangle],\end{aligned} \qquad (45)$$

where

$$\Psi_{\alpha\beta} = \sum_{li}(\partial\Phi/\partial x_{\alpha li})x_{\beta li}. \qquad (46)$$

If we formulate the potential as a function of the squared pair distances

$$\rho_{limj} = |\mathbf{r}_{li} - \mathbf{r}_{mj}|^2, \qquad (47)$$

which does not imply pairwise additivity, the second term on the right-hand side of (45) can be replaced by

$$\begin{aligned}&\sum_{li,\,mj} x_{\delta li}(\partial^2\Phi/\partial x_{\gamma li}\,\partial x_{\alpha mj})x_{\beta mj} \\ &\quad = 4\sum_{li<l'i'}\sum_{mj<m'j'}(\partial^2\Phi/\partial\rho_{lil'i'}\partial\rho_{mjm'j'}) \\ &\qquad \times x_{\alpha mjm'j'}x_{\beta mjm'j'}x_{\gamma lili'i'}x_{\delta lil'i'} + \delta_{\alpha\gamma}\Psi_{\beta\delta},\end{aligned} \qquad (48)$$

where (46) becomes

$$\Psi_{\beta\delta} = 2\sum_{li<l'i'}(\partial\Phi/\partial\rho_{lil'i'})x_{\beta ili'l'}x_{\delta ili'l'} = \Psi_{\delta\beta}. \qquad (49)$$

Here, the components of the vectors $\mathbf{r}_{lil'i'} = \mathbf{r}_{li} - \mathbf{r}_{l'i'}$ have been introduced and a $<$ under a summation sign means that no atom pair must be counted twice. If we then use (42) in the form $\langle\Psi_{\beta\delta}\rangle = nNkT\delta_{\beta\delta} - VP_{\beta\delta}$ and add and subtract a term $nNkT\delta_{\alpha\beta}\delta_{\gamma\delta}$, we can arrange the terms according to their symmetry properties:

$$\begin{aligned}&(\partial^2 A/\partial S_{\alpha\beta}\partial S_{\gamma\delta}) \\ &\quad = nNkT(\delta_{\beta\gamma}\delta_{\alpha\delta} + \delta_{\alpha\gamma}\delta_{\beta\delta} + \delta_{\alpha\beta}\delta_{\gamma\delta}) \\ &\qquad + \Bigg\langle 4\sum_{li<l'i'}\sum_{mj<m'j'}(\partial^2\Phi/\partial\rho_{lil'i'}\partial\rho_{mjm'j'}) \\ &\qquad \times x_{\alpha mjm'j'}x_{\beta mjm'j'}x_{\gamma lil'i'}x_{\delta lil'i'}\Bigg\rangle \\ &\qquad - (1/kT)[\langle\Psi_{\alpha\beta}\Psi_{\gamma\delta}\rangle - \langle\Psi_{\alpha\beta}\rangle\langle\Psi_{\gamma\delta}\rangle] \\ &\qquad - nNkT\delta_{\alpha\beta}\delta_{\gamma\delta} - \delta_{\alpha\gamma}VP_{\beta\delta}.\end{aligned} \qquad (50)$$

The first term on the right-hand side has full Cauchy symmetry, *i.e.* it is invariant under any permutation of its indices. The second term, within $\langle\,\rangle$, has full Cauchy symmetry if the potential is pairwise additive, otherwise it has the same symmetry as the third and fourth terms, which are invariant under the interchanges of α with β, γ with δ and $\alpha\beta$ with $\gamma\delta$. The last term is invariant only under the interchange of α with γ and β with δ. Another noteworthy symmetry property holds for the second, third and fourth terms. If we symmetrize any of them with respect to the second and fourth indices, it is automatically symmetrized with respect to the first and third indices and *vice versa*. It then has full Cauchy symmetry too. Symmetrizing $C_{\alpha\beta\gamma\delta}$ with respect to its second and fourth indices also symmetrizes it with respect to its first and third indices. It does, however, not endow it with full Cauchy symmetry because of the last term.

A result similar to (50) was obtained by Squire, Holt & Hoover (1969) but only for a pairwise additive potential and the derivation of the ideal-gas part was not given in that paper. Note that (50) is valid for any many-body potential, which is very important since the commonly used energy terms associated with bond angles, dihedral angles and improper torsions are three- and four-body terms.

It should be mentioned that (14) is also called the (isothermal) 'displacement-gradient elasticity tensor' in the literature, especially when the terms 'elasticity tensor' or 'elastic constants' or 'elastic moduli' are reserved for

$$C^E_{\alpha\beta\gamma\delta} := (1/V)(\partial^2 A/\partial E_{\alpha\beta}\partial E_{\gamma\delta}), \qquad (51)$$

which is analogous to (14), but with the transformation matrix (16) replaced by the symmetric strain tensor

$$\begin{aligned}E_{\beta\gamma} &= \tfrac{1}{2}(S_{\alpha\beta}S_{\alpha\gamma} - \delta_{\beta\gamma}) \\ &= \tfrac{1}{2}[\partial u_\beta/\partial x_\gamma + \partial u_\gamma/\partial x_\beta + (\partial u_\alpha/\partial x_\beta)(\partial u_\alpha/\partial x_\gamma)].\end{aligned} \qquad (52)$$

See *e.g.* Weiner (1983). The two tensors are related by

$$C_{\alpha\beta\gamma\delta} = C^E_{\alpha\beta\gamma\delta} - \delta_{\alpha\gamma}P_{\beta\delta}, \qquad (53)$$

i.e. $C^E_{\alpha\beta\gamma\delta}$ is given by the first four tems on the right-hand side of (50), divided by V, and has at most 21 independent components. After symmetrization with respect to its second and fourth indices, it has full Cauchy symmetry and at most 15 independent components. For more fluctuation formulae for isothermal or adiabatic elasticity tensors, see *e.g.* Ray (1988).

References

LUCKAS, M., LUCAS, K., DEITERS, U. & GUBBINS, K. E. (1986). *Mol. Phys.* **57**/2, 241–253.

RAY, J. R. (1988). *Comput. Phys Rep.* **8**, 109–152.

SQUIRE, D. R., HOLT, A. C. & HOOVER, W. G. (1969). *Physica (Utrecht)*, **42**, 388–397.

WEINER, J. H. (1983). *Statistical Mechanics of Elasticity*. New York: Wiley.